Coexisting single-particle and collective excitations in ^{70}As

R. A. Haring-Kaye, R. M. Elder, J. Döring, S. L. Tabor, A. Volya, P. R. P. Allegro, P. C. Bender, N. H. Medina, S. I. Morrow, J. R. B. Oliviera, and V. Tripathi

Phys. Rev. C **92**, 044325 — Published 26 October 2015

DOI: 10.1103/PhysRevC.92.044325

Coexisting single-particle and collective excitations in ^{70}As

R. A. Haring-Kaye,[1] R. M. Elder,[1] J. Döring,[2] S. L. Tabor,[3] A. Volya,[3] P. R. P. Allegro,[4] P. C. Bender,[3] N. H. Medina,[4] S. I. Morrow,[5] J. R. B. Oliviera,[4] and V. Tripathi[3]

[1]*Department of Physics and Astronomy, Ohio Wesleyan University, Delaware, Ohio 43015, USA*

[2]*Bundesamt für Strahlenschutz, D-10318 Berlin, Germany*

[3]*Department of Physics, Florida State University, Tallahassee, Florida 32306, USA*

[4]*Instituto de Física, Universidade de São Paulo, São Paulo, Brazil*

[5]*Department of Physics, Houghton College, Houghton, New York 14744, USA*

Abstract

High-spin states in ^{70}As were studied using the ^{55}Mn(^{18}O,3n) fusion-evaporation reaction at a beam energy of 50 MeV. Prompt γ-γ coincidences were measured using the Florida State University Compton-suppressed Ge array consisting of three Clover detectors and seven single-crystal detectors. A reinvestigation of the known level scheme resulted in the addition of 32 new transitions and the rearrangement of 10 others. The high-spin decay pattern of yrast negative-parity states was modified and enhanced extensively. Spins were assigned based on directional correlation of oriented nuclei ratios. Lifetimes of seven excited states were measured using the Doppler-shift attenuation method. The $B(E2)$ rates inferred from the lifetimes of states in the yrast positive-parity band imply substantial collectivity, in agreement with the results of previous studies. Substantial signature splitting and large alternations in the $B(M1)$ strengths were observed in this band as well, supporting the interpretation of an aligned $\pi g_{9/2} \otimes \nu g_{9/2}$ intrinsic configuration for this structure beginning at the lowest 9^+ state. Large-scale shell-model calculations performed for ^{70}As reproduce the relative energy differences between adjacent levels and the $B(M1)$ rates in the yrast positive-parity band rather well, but underestimate the $B(E2)$ strengths. The $g_{9/2}$ orbital occupancies for the lowest 9^+ state predicted by the shell-model calculations provide additional evidence of a stretched $\pi g_{9/2} \otimes \nu g_{9/2}$ configuration for this state.

PACS numbers: 21.10.Tg, 23.20.Lv, 27.50.+e

I. INTRODUCTION

Nuclei in the mass $A \approx 70$ region continue to provide a fruitful testing ground for exploring the interplay between single-particle and collective modes of excitation. The valence space for both protons and neutrons lies in a transitional region of the f-p-g shell, between the spherical shell closure at $N = Z = 28$ and a locus of strongly-deformed nuclei in the middle of this shell. The valence nucleons can also polarize the core shape, since the potential-energy surfaces of these nuclei tend to be insensitive to both the quadrupole deformation β_2 and triaxiality γ shape parameters. In particular, quasiparticle (qp) occupation of the $g_{9/2}$ orbital is well known to drive the nucleus toward increased collectivity and deformation [1]. Investigating the microscopic framework of these behaviors provides a challenging test of contemporary shell-model predictions, especially due to the large number of basis states required in the calculations.

Odd-odd nuclei in this region provide a laboratory particularly well-suited to investigate the competition between single-particle and collective degrees of freedom. Single-particle excitations are manifested clearly at low excitation energy by a complex spectrum of excited states due to the many different 2-qp states that can be generated by the unpaired nucleons. However, this picture can quickly evolve to one in which regular rotational structures are observed with increasing excitation energy and spin, usually due to qp occupation of the high-j $g_{9/2}$ "intruder" orbital. Occupation of this orbital is, of course, sensitive to the Fermi level of valence protons and neutrons, so a precise understanding of the single-particle energy spectrum (and its dependence on the underlying core shape) is very important for an accurate description of how nuclear structure changes with N and Z.

The proton-rich, odd-odd As isotopes provide a clear example of the transitional nature of this mass region, and illustrate how competing single-particle and collective behaviors depend sensitively on nucleon number. The excited states of ^{68}As systematically show irregular spacings, even at high spin, characteristic of non-collective, single-particle excitations [2]. On the other hand, evidence of rotational structures associated with both positive- and negative-parity configurations was observed above an excitation energy of about 800 keV in ^{72}As, one of which was associated with the $\pi g_{9/2} \otimes \nu g_{9/2}$ configuration [3, 4].

The ^{70}As nucleus, lying intermediate between ^{68}As and ^{72}As, might be expected to show strong competition between single-particle and collective behavior. At low spin, the excited

states and their decays were observed to form a complex network typical of 2-qp spin coupling [5–7]. Early studies of high-spin states using heavy-ion reactions discovered states suggested to be based on the $\pi g_{9/2} \otimes \nu g_{9/2}$ configuration [8], and later observed evidence for the onset of a rotational band based on this configuration [9]. The most recent high-spin study [10] extended this band up to a (19^+) state at 8941 keV, and found a signature-partner band up to a (14^+) state at 4900 keV. Curiously, the normalized energy differences between adjacent states (indicative of signature splitting) in these signature-partner bands do not follow the same pattern as what is typically observed for yrast positive-parity bands in this mass region [11]. Usually, states with even spin lie relatively lower in energy than the odd-spin ones below spin $J \approx 9$, with small amplitudes associated with this alternating pattern. Above spin $J \approx 9$, there is a reversal in the pattern, such that the odd-spin states lie relatively lower in energy than the even-spin ones with an increasing amplitude of the alternating pattern with spin. Such behavior has been observed in the yrast positive-parity band of ^{72}As [3], and can be explained [12] by a predominance of qp realignment (collective rotation) below (above) $J = 9$, the maximum spin of two unlike $g_{9/2}$ nucleons. However, a phase change in the signature splitting pattern of the yrast positive-parity band has not been observed in ^{70}As, which has been attributed to a fully-aligned $\pi g_{9/2} \otimes \nu g_{9/2}$ configuration and a deformed prolate core shape at the onset of this band [10]. Further theoretical explorations of this rather unique behavior in ^{70}As could help to understand its microscopic underpinnings. Additionally, quantitative estimates of the degree of collectivity with spin throughout this band from measured $B(E2)$ rates would be especially useful in testing the assertion of fully aligned, collective states at and above the 9^+ state. However, so far lifetimes have only been measured for the 8^+ and 9^+ states using the γ-ray lineshape method [13], and the 11^+ and 13^+ states using the Doppler-shift attenuation method [14] (with the lifetime of the 13^+ state representing an upper-limit only).

A high-spin, negative-parity band with signature $\alpha = 0$ was also discovered recently, with energy spacings indicative of rotational behavior [10]. A similar sequence was observed in ^{72}As based on a 6^- state at 834 keV [3], along with a signature $\alpha = 1$ partner band and several linking transitions between the two bands. However, unlike the corresponding negative-parity band structure in ^{72}As, there was only one high-spin $(13^-) \rightarrow (11^-)$ transition observed in the $\alpha = 1$ sequence in ^{70}As, and only one linking transition discovered between the two signature partners. Although the yrast negative-parity states in ^{68}As do

not follow a rotational pattern, high-spin states grouped into bands include those with $J = 7$ and 9, as they do in ^{72}As. Therefore, it seems likely that such odd-spin negative-parity states should also exist in ^{70}As. Finding these "missing" states could provide insight into the underlying structure properties associated with the negative-parity states, and how they fit within the contrasting picture of the rather irregular $E2$ transition energies associated with the yrast negative-parity sequences in ^{68}As [2] and the much more regular ones observed in ^{72}As [3].

An important goal of the present work was thus to reinvestigate the level scheme of ^{70}As to search for new negative-parity states, and to verify the additions at high spin put forth in Ref. [10]. In order to address the unresolved questions concerning the irregular signature-splitting pattern in the yrast positive-parity states, which may be attributed to the underlying shape and degree of collectivity, the lifetimes of several high-spin states were measured using the Doppler-shift attenuation method (DSAM). These results could then be augmented by the recent lifetime measurements of the yrast 8^+ and 9^+ states (which are too long to be measured by the DSAM) to provide a fuller picture of the evolution of collectivity with spin in this band structure. Additionally, large-scale shell-model calculations were performed to test how well they reproduce the experimental energy spectrum for the positive-parity high-spin states, as well as the $E2$ and $M1$ transition rates between them.

II. EXPERIMENTAL AND ANALYSIS METHODS

High-spin states in ^{70}As were populated by the ^{55}Mn(^{18}O,3n) fusion-evaporation reaction at a beam energy of 50 MeV using the John D. Fox Superconducting Accelerator Facility at Florida State University (FSU). The 3n channel comprised approximately 12% of the total reaction cross section and represented the third-largest yield among several reaction products. The ^{55}Mn target had a thickness of 611 μg/cm^2 and was evaporated on to a 15 mg/cm^2 ^{197}Au backing to stop all recoils produced from the reaction and to allow for an analysis of Doppler-shifted γ-ray line shapes using the DSAM.

The γ rays emitted from the reaction products were detected by an array of ten Compton-suppressed Ge detectors. Three Clover detectors and two single-crystal detectors were placed at 90° relative to the beam axis, and two (three) single-crystal detectors were placed at 35° (145°). Approximately 2.3×10^8 prompt γ-γ coincidences were recorded by the array

under the condition that each two-fold (or higher) multiplicity event occurred within a time window of 100 ns. These data were then sorted into a variety of γ-γ coincidence matrices with a dispersion of 0.8 keV/channel. Both the sorting and analysis of the γ-ray spectra were performed using GNUSCOPE, a γ-spectrum analysis software package developed at FSU [15, 16].

The γ-ray coincidences used to verify and enhance the existing ^{70}As level scheme were investigated mostly with background-subtracted spectra projected from matrices of coincidences among the 90° detectors, in order to minimize Doppler shifting. For the DSAM lifetime analysis, Doppler-shifted line shapes measured at 35° (145°) were obtained from background-subtracted spectra projected from matrices consisting of coincidence events between any 35° (145°) detector and all other detectors in the array in order to maximize the measurement statistics. This choice was also motivated by the fact that only clean gates on low-lying transitions (i.e. those that did not show evidence of Doppler shifting) were used to project 35° and 145° spectra. Approximately 3.6×10^7 (4.6×10^7) coincidence pairs were sorted in the matrix that incorporated coincidences between any 35° (145°) detector and all other detectors in the array. Additional details about the DSAM analysis method are discussed in Sec. IV.

Transition energies were determined by measuring the line centroids for the decays in as many clean gates as possible in the 90° coincidence spectra and taking a weighted average (based on the uncertainties of individual measurements). Preliminary energy calibrations were obtained from an ^{152}Eu source, then modified to include a broader energy range based on the known energies of several clean γ-ray lines produced in beam. The γ-ray intensities were first determined at 90° and then corrected for angular distribution effects using theoretical a_2 and a_4 coefficients determined from the spin change of the transition. These coefficients were then used to deduce A_0, the angle-independent first-order term in the series of Legendre polynomials that describe the experimental intensities as a function of observation angle. Lastly, the A_0 values were normalized to the one obtained for the 788.2-keV transition, resulting in a final relative intensity I_γ for each transition. Intensities for transitions with energy $E_\gamma > 200$ keV were determined either through clean gates on transitions below the lines of interest or from the total projection of 90° detector coincidences. Due to a low-energy discriminator threshold problem with some of the 90° detector electronics, the intensities of transitions with energy $E_\gamma < 200$ keV were determined from a γ-singles

spectrum recorded by one of the 35° detectors, with the results corrected to compensate for angular distribution effects as described above. The relative efficiency of the detectors as a function of E_γ was determined from the known intensities of a ^{152}Eu calibration source [17] and a standard logarithmic parameterization for Ge detectors. All measured γ-ray energies and intensities for ^{70}As are given in Table I.

Spin changes were measured for as many transitions in ^{70}As as possible based on DCO ratios, defined according to:

$$R_{\rm DCO} = \frac{I_\gamma(\text{at } 35^\circ, 145^\circ;\ \text{gated by } \gamma_{\rm G} \text{ at } 90^\circ)}{I_\gamma(\text{at } 90^\circ;\ \text{gated by } \gamma_{\rm G} \text{ at } 35^\circ, 145^\circ)}. \quad (1)$$

In order to increase the statistics of the DCO ratio measurement, the analysis was performed using a matrix constructed to exploit the angular symmetry of the FSU Ge array, in which both 35° and 145° detector events were sorted against only the 90° detector events. Based on the geometry of the array, if the gate γ_G represents one or more stretched electric quadrupole ($E2$) transitions, then the DCO ratios for stretched $E2$ transitions as well as for $\Delta J = 0$ transitions are expected to be approximately unity, while $\Delta J = 1$ transitions yield ratios of about 0.5 if the mixing ratio δ is small [18]. Most DCO ratios were measured by gating on stretched $E2$ decays, while a few others were determined by gating on known $E1$ transitions assuming $\delta = 0$. All such measurable ratios are shown in Table I and in most cases reflect weighted averages (based on the measurement uncertainty) of the results obtained from two or more gates.

III. THE LEVEL SCHEME

The level scheme of ^{70}As based on the present work is shown in Fig. 1. All of the states and transitions shown in Ref. [9] have been verified. Some of the additional low-lying states reported in Ref. [7] were also observed. However, a significant rearrangement of the high-spin level scheme compared to that shown in Ref. [10] has been performed, based primarily on the measured γ-γ coincidence relations and relative γ-ray intensities. In all, 32 new transitions were assigned to ^{70}As in this work, and 10 others have had their placement rearranged compared to the most recent work [10]. The supporting evidence for these changes and other new additions to the level scheme are discussed in detail below.

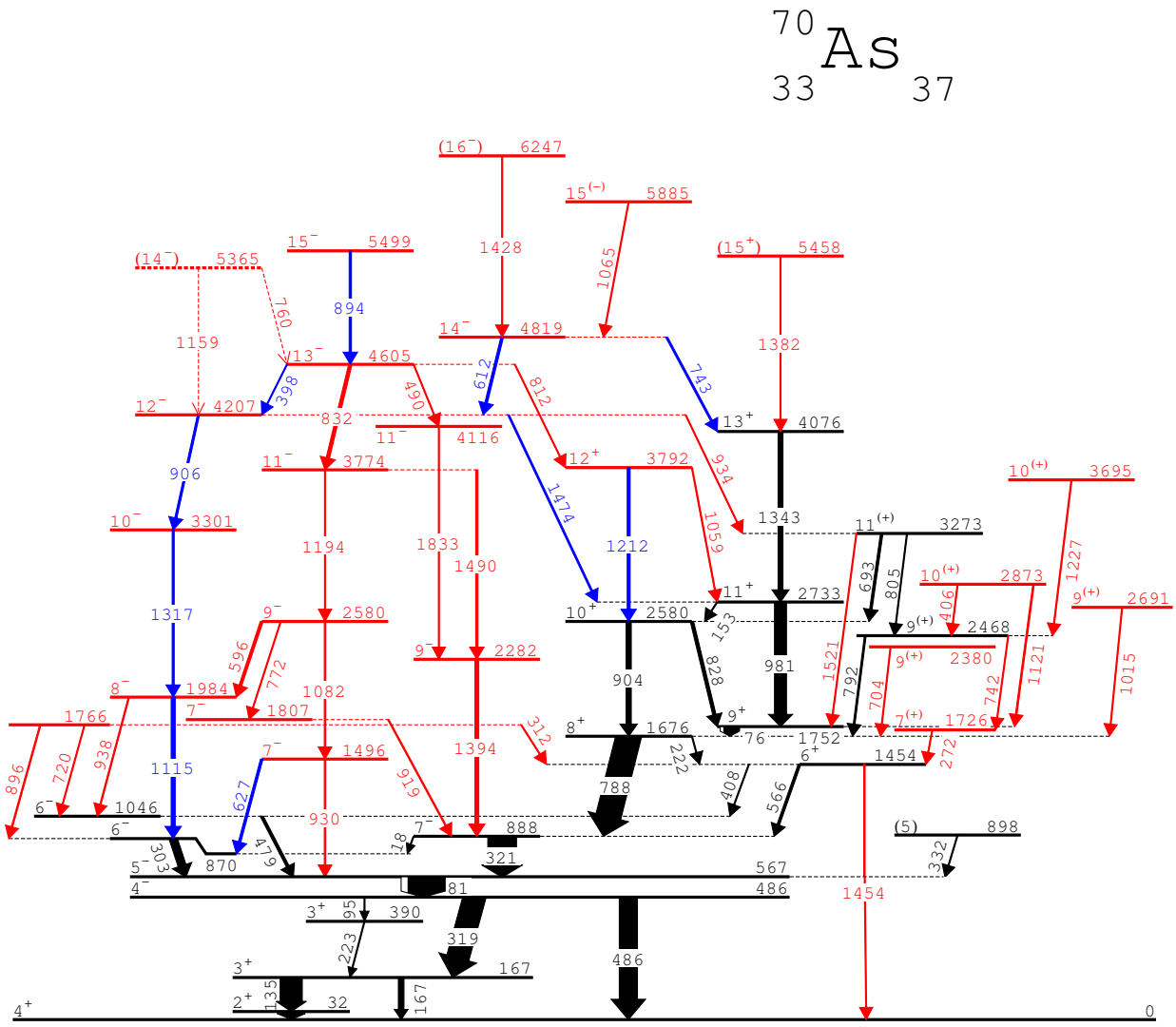

FIG. 1: (Color online) The level scheme of ^{70}As as deduced from the present work. Transitions with energies less than 76 keV have not been observed directly but are included for completeness. The vertical energy scale has been compressed by a factor of 1.5 above an excitation energy of 567 keV. Transitions and states shown in red (light grey) are new to this work, while those indicated in black have been verified from previous investigations. Transitions with rearranged placements compared with a prior high-spin study [10] are shown in blue (light grey).

A. Low-lying states

The low-lying states of ^{70}As below about 2 MeV have been established from the β^+ decay of ^{70}Se [5], $(p, n\gamma)$ reactions [6, 7], and heavy-ion reactions [8–10]. Most of the low-lying

states observed previously through heavy-ion reactions were verified in this work, with the exception of the 933.4-, 1809.2-, and 2030.2-keV levels reported in Ref. [8].

Most of the spin-parity assignments of the low-lying states were taken directly from Ref. [7]. In some cases, it was possible to unambiguously assign spins and parities for states that previously only had tentative assignments, based on the discovery of new linking transitions. For example, the 1454.4-keV state first reported in Ref. [9] was assigned a spin of either $J = 6, 7$, or 8 (without a suggested parity assignment) based on the properties of the decays to and from this state. In this work, we have discovered a weak 1454.2-keV transition from this state to the ground state, which has a firm spin-parity of 4^+ [19, 20]. This uniquely establishes the spin-parity of the 1454.2-keV state as $J^\pi = 6^+$ based on transition probability arguments. Similarly, the 1045.9-keV state, listed with $J^\pi = 6^{(+)}$ in Ref. [9], has been assigned $J^\pi = 6^-$ in this work based on a newly-observed 938.4-keV $\Delta J = 2$ transition (which almost certainly has $E2$ character) to this state from an 8^- parent state at 1984.2 keV.

The new 6^+ assignment for the 1454.2-keV state and the recent mean lifetime measurement of the 1676.0-keV 8^+ state [13] strongly support $E2$ multipolarity for the 221.8-keV transition between these levels based on transition probability arguments, confirming the positive-parity assignment for the 1676.0-keV state [9]. The known $E1$ character of the 788.2-keV transition, the $E2$ nature of the 321.1-keV transition, and the firm spin assignments of their corresponding parent states [9] therefore allows an unambiguous spin-parity assignment of 7^- (5^-) to the 887.8-keV (566.7-keV) state. These assignments are consistent with the implications of the measured upper limit for the half-life of the 567-keV state ($T_{1/2} < 2$ ns) [9]. This lifetime limit strongly favors an $M1/E2$, rather than $E1$, multipolarity for the 81-keV transition based on the resulting lower limits placed on the corresponding $B(E1)$ and $B(E2)$ strengths, and thus a negative-parity assignment for the 567-keV parent state given the firm 4^- assignment for the 486-keV level [9].

B. High-spin positive-parity states

Excited states at 1676.2 and 1752.3 keV were first observed from heavy-ion fusion-evaporation reactions [8, 9], and were assigned $J^\pi = 8^+$ and 9^+, respectively, based on angular distribution data, linear polarization measurements, and excitation function argu-

ments [9]. At the time of their discovery, it was speculated that these states were associated with the $\pi g_{9/2} \otimes \nu g_{9/2}$ intrinsic configuration [8, 9]. High-spin states were also observed up to a (13^+) state at 4075.7 keV based on the same intrinsic configuration [9]. More recently, yrast positive-parity states were extended up to a (19^+) state at 8941 keV and a (14^+) state at 4900 keV as part of an even- and odd-spin band structure indicative of a coupled rotational sequence with pronounced signature splitting [10]. Although we observed a 1212.0-keV line belonging to the signature $\alpha = 0$ sequence, which probably corresponds to the 1210-keV decay shown in Ref. [10], we could neither confirm its placement nor observe any of the other new transitions reported above the 13^+ (10^+) state in the $\alpha = 1$ $(\alpha = 0)$ sequence. Instead, our data suggest the addition of a single 1381.8-keV (1212.0-keV) transition above the 13^+ (10^+) state in the $\alpha = 1$ $(\alpha = 0)$ sequence, extending this band up to a (15^+) (12^+) state at 5458.1 keV (3792.0 keV). This new construction is further supported by the observation of a 1058.9-keV linking transition between the new 12^+ state and the known 11^+ state at 2733 keV [9], and the discovery of a new high-spin negative-parity structure that feeds the 12^+ state through a 812.1-keV transition (see Fig. 1 and Sec. III C). Figure 2 shows a portion of the background-corrected 90° γ-ray spectrum measured in coincidence with the 788.2- and 980.7-keV transitions, showing evidence for the new construction of the high-spin positive-parity yrast states.

Several additional states were observed to feed directly to the yrast positive-parity levels (and to each other) within an excitation energy range of about 1700-3700 keV (see Fig. 1). Most of the transitions from these states were strong enough to support spin assignments based on DCO ratio measurements. A tentative assignment of positive parity has been suggested for these states due to the strong decay flux to the yrast positive-parity levels.

C. High-spin negative-parity states

As mentioned in Sec. I, an even-spin negative-parity band based on the known $6^{(-)}$ state at 869.6 keV [9] was shown in the most recent ^{70}As level scheme, extending up to a (14^-) state at 5679 keV [10]. Our measured coincidence relations and relative intensity measurements suggest a different ordering of the lowest three members of this band, as indicated in Fig. 1. This new arrangement is further supported by linking transitions found to/from the new 8^- state at 1984.2 keV and the new 12^- state at 4207.0 keV. Spin-parity

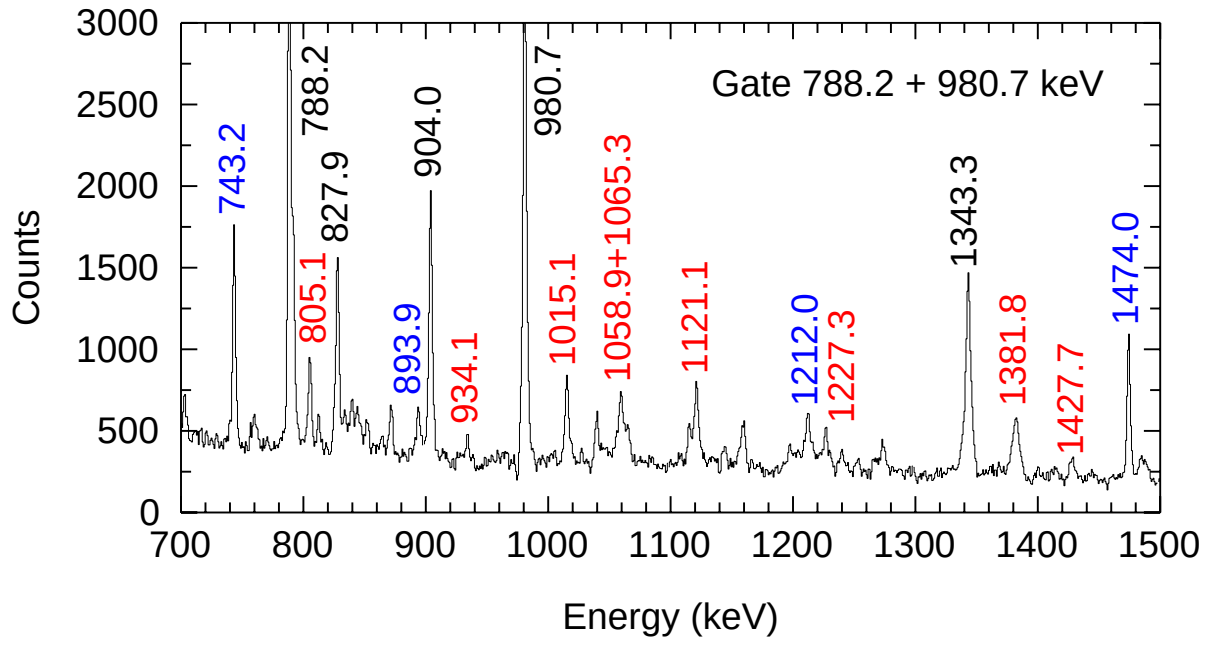

FIG. 2: (Color online) A portion of the 90° background-subtracted coincidence spectrum obtained by gating on the 788.2- and 980.7-keV γ rays. New (Rearranged) transitions in the ^{70}As level scheme, as determined from this work, have their energies labeled in red (blue) or light grey.

assignments in this band are proposed on the basis of DCO ratio measurements and the likely $E2$ multipolarity of the prompt $\Delta J = 2$ transitions that were observed. Figure 3 shows a portion of the background-corrected 90° γ-ray spectrum measured in coincidence with the 302.8-keV transition, indicating the transitions in this band.

The 1475-keV decay that was proposed to be the highest-lying transition in this negative-parity band [10] has been rearranged as a new $12^- \rightarrow 11^+$ transition of energy 1474.0 keV, in agreement with our observed coincidence relations (see Fig. 4), the energy difference between these two states, and the measured DCO ratio for this transition (see Table I). As illustrated in Fig. 4, the 1474-keV transition is not in coincidence with a 1317-keV line, as it would be in the previous level scheme construction [10]. The strong peaks observed near 906 and 1115 keV in this spectrum are very likely due to coincidences between the known [21] 1474.8-keV decay and transitions of energy 905.3 and 1112.7 keV in the ground-state band of ^{70}Ge, a strong byproduct of the reaction used in our experiment. Note that ^{70}Ge was also produced significantly [22] in the ^{46}Ti(^{28}Si,3pn) reaction used to populate ^{70}As in Ref. [10], and thus the same contaminating lines from ^{70}Ge would likely have been observed

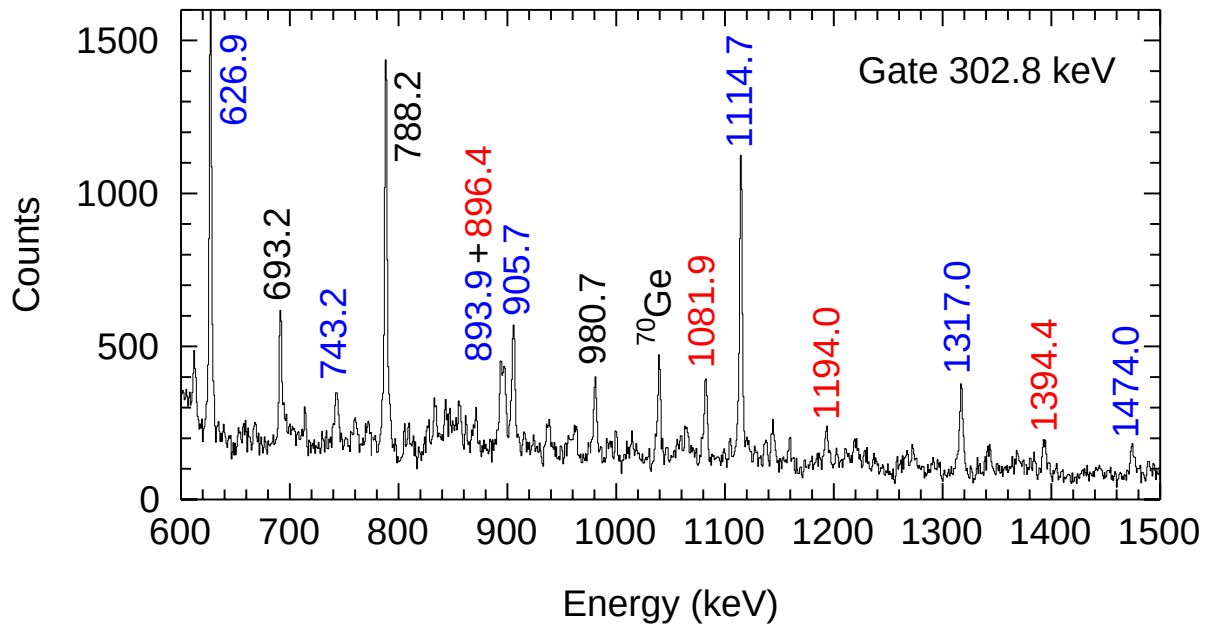

FIG. 3: (Color online) A portion of the 90° background-subtracted coincidence spectrum obtained by gating on the 302.8-keV γ ray. New (Rearranged) transitions in the ^{70}As level scheme, as determined from this work, have their energies labeled in red (blue) or light grey.

in a gate on the 1474-keV decay from that data set as well.

Our coincidence data also revealed two new odd-spin decay sequences that almost certainly have negative parity based on the likely $E2$ character of the observed $\Delta J = 2$ decays (established from measured DCO ratios) that depopulate these states. One sequence appears to be based on the 5^- state at 566.7 keV, while the other seems to begin at the 7^- state at 887.8 keV. Interestingly, both sequences share a common 11^- state at 3773.5 keV as they progress to higher spins, although a second, more weakly populated, 11^- state was found at 4115.5 keV that decays by a weak 1832.8-keV transition to the 9^- state at 2282.2 keV. Many of the transitions associated with these odd-spin negative-parity sequences (most of which have not been placed in previous studies) are shown in Fig. 3.

Above an excitation energy of about 4 MeV, the observed negative-parity sequences appear to fragment and split among multiple structures. Some of the transitions associated with these structures were previously placed as part of a decay sequence that funneled to the 11^+ yrast state [10], but this construction was inconsistent with our observed coincidence relations. Unfortunately, the generally poor statistics associated with the decays of

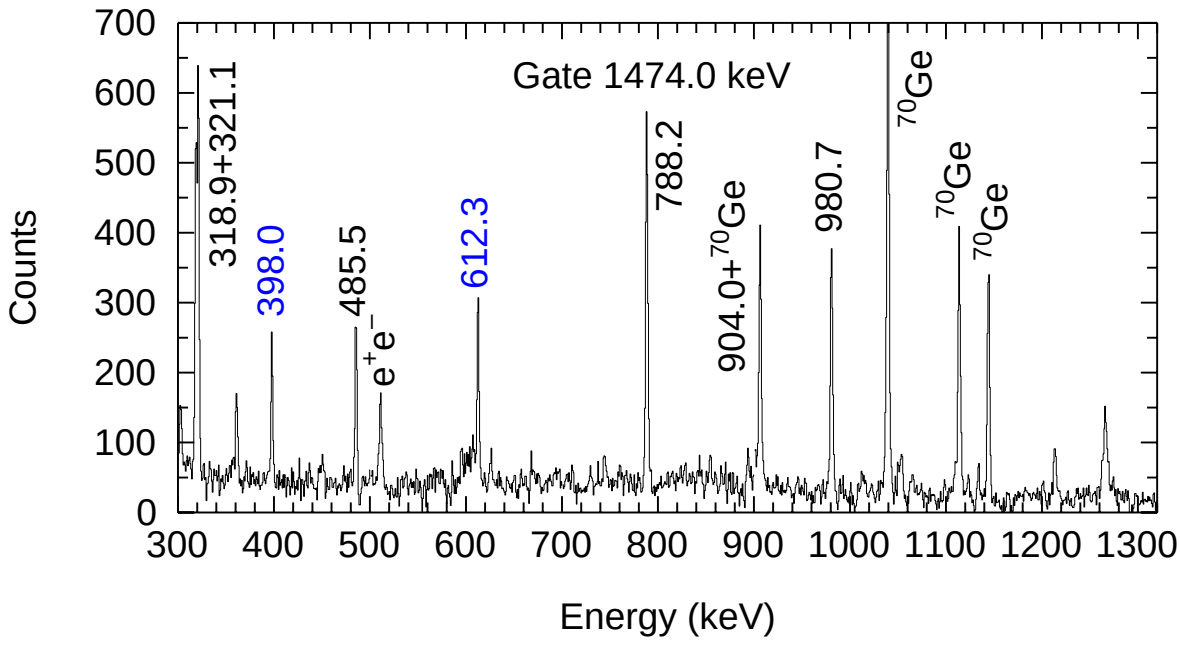

FIG. 4: (Color online) A portion of the 90° background-subtracted coincidence spectrum obtained by gating on the 1474.0-keV γ ray. Transitions with rearranged placements in the ^{70}As level scheme, as determined from this work, have their energies labeled in blue (light grey).

these higher-lying states made it difficult to find any band structures, although the effective lifetime measurement of the 14^- state at 4819.4 keV (see Sec. IV) seems to suggest the onset of increased collectivity (and thus rotational structures) in this spin range.

IV. LIFETIME MEASUREMENTS

Lifetimes of seven excited states were measured by applying the DSAM to the experimental line shapes of coincident γ rays detected at 35° and 145°. A comparison between the decay time of the recoiling nuclei and the slowing down in a thin target with a backing foil was carried out using the simulation code FITS [18], which integrates over the thickness of the target with backing and accounts for evaporation of charged particles by determining a Gaussian distribution of recoil velocities (with a width that is 10% of the kinematic mean) at the time of decay. It corrects for direct feeding from up to four known higher-lying states and side feeding from one unknown state, as well as for finite detector solid angle and resolution, and the changing (energy-dependent) reaction cross sections due to the beam slowing down through the target and backing. The nuclear and electronic stopping powers

were obtained from the SRIM software [23].

By varying the lifetime of the parent state of interest, a set of theoretical line shapes for each associated transition was produced and compared with the measured Doppler-shifted spectrum at 35° and 145° to find the best fit. The lifetime associated with the theoretical line shape that best fit the experimental one through a χ^2 minimization was taken as the lifetime of the parent state. The limits of uncertainty in the individual lifetimes were taken to be the lifetime values above and below the best-fit value that increased the minimum χ^2 value by one unit, and thus represent an estimate of the statistical uncertainties (one-standard deviation) in the lifetime measurements [24]. The accepted lifetime values were determined from a weighted average (based on the estimated uncertainties) of the individual lifetimes whenever measurements were possible at both angles (see Table II). If a measurement could only be performed at one angle, then the accepted lifetime (and its uncertainty) came directly from the measurement at that angle. The uncertainties in the accepted lifetimes representing a weighted average were deduced from the reciprocal square root of the sum of the individual weights, with each individual weight given by the reciprocal square of the measurement uncertainty [25].

All line shapes were obtained from coincidence spectra of transitions gated from below the transition of interest. It was not possible to obtain reliable line shapes from spectra gated from above the transitions of interest due to either limited statistics or interference from contaminant reaction products. Effective lifetimes, which do not include feeding corrections, were first determined for each line shape with adequate statistics. Whenever possible, an accepted effective lifetime of each state was determined from the weighted average (based on the individual uncertainties) of the results obtained at 35° and 145°. All line shapes for which the direct feeding pattern to the parent state was known were then refit with feeding corrections, with the exception of those from the highest fitted transition in each decay sequence, where only an upper-limit effective lifetime could be obtained.

The feeding corrections used the effective lifetime of the state (or possibly multiple states) immediately above and one side-feeding state to populate the state of interest. Side-feeding times were determined from a procedure adopted for a similar heavy-ion reaction used to populate high-spin states in ^{71}As [26], where the highest measurable state for which a mean lifetime can be determined is given a short side-feeding time, with an increase of about 0.04 ps per MeV of de-excitation. This choice was also motivated by a rigorous theoretical study

of side-feeding times in this mass region [27], as well as the measured results for ^{82}Sr [28] and ^{83}Y [29]. The present study incorporated a side-feeding time of 0.10 ps for the 13^+ state in ^{70}As, which on average provided line-shape fits with the lowest χ^2 at both detector angles for a given assumed mean lifetime of this state. All other side-feeding times were then based on this value using the method described above due to the insensitivity of the line-shape fits to the side-feeding time for states below the 13^+ level. Modeling the side-feeding times in this fashion leads to a side-feeding time of 0.15 ps for the yrast 11^+ state, consistent with the value of 0.2 ps used for this state in a previous DSAM measurement [14]. In order to test the sensitivity of the mean lifetime on the side-feeding time in the simulation, the estimated side-feeding time was varied for the yrast 10^+ and 11^+ states. As an example, doubling the side-feeding time resulted in a 13% average reduction of the associated mean lifetime. Therefore, it was determined that the measured mean lifetimes were mostly insensitive to the side-feeding time, probably because the side-feeding intensity was typically a small fraction of the total feeding intensity.

Of the seven lifetimes measured in this work, four represent upper-limits based on effective lifetimes and three correspond to mean lifetimes. No additional measurements were possible due to either the lack of a Doppler-shifted component to the observed line shape, limited statistics, or contamination from other reaction products. In particular, the line shapes corresponding to decays from yrast negative-parity states below the 12^- state at 4207.0 keV did not show a Doppler-shifted component, possibly indicating rather non-collective behavior associated with these states.

Five of the seven lifetimes represent new measurements, and the mean lifetime of the 13^+ state has been determined for the first time. Although our measured mean lifetime of the 13^+ state agrees with the upper-limit constraint determined previously [14], the mean lifetime of the yrast 11^+ state deduced in this work indicates a slight disagreement with the previous measurement [14] (see Table II). The line-shape fits to the 980.7- and 1343.3-keV transitions at both 35° and 145°, used to infer the mean lifetimes of the yrast 11^+ and 13^+ states, respectively, are shown in Fig. 5.

A particularly interesting feature of the 1343.3-keV line shape is that it contains both a significant shifted and unshifted component, indicative of both a fast and slow component of the feeding pattern that are competing favorably toward the population of the 13^+ state. This seems to imply a more complex feeding pattern for the 13^+ state than just the simple

fast intraband feeding shown in Ref. [10], and tends to support the proposed changes to the feeding pattern indicated in Fig. 1.

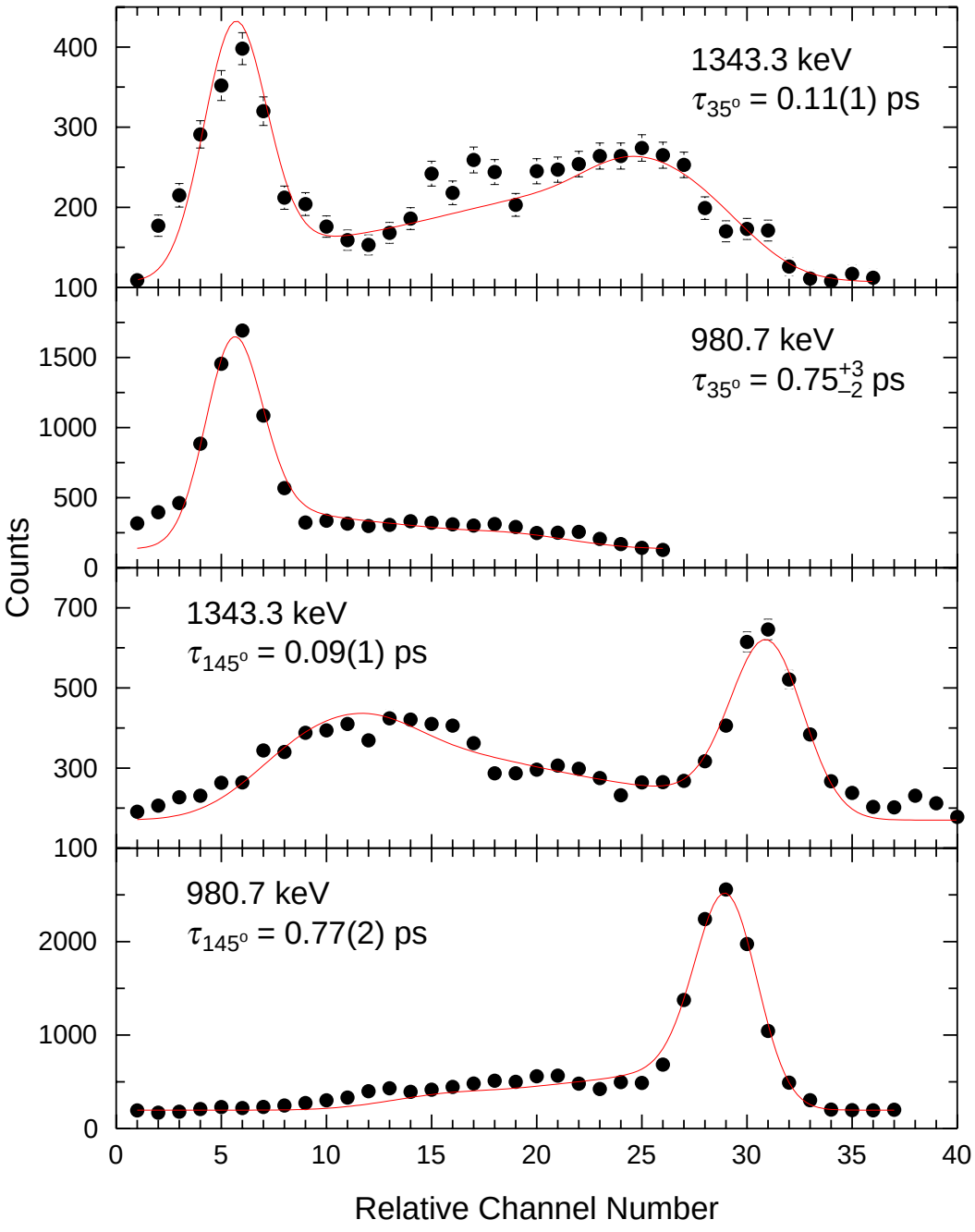

FIG. 5: (Color online) Fits to the 35° and 145° line shapes of the 980.7- and 1343.3-keV transitions. The simulated line shapes that best fit the experimental ones with the given parent-state lifetimes are indicated by the solid curves. Some error bars are smaller than the symbol size.

All measured lifetimes in ^{70}As, including those determined in Refs. [13] and [14], are

given in Table II, along with reduced electric quadrupole transition strengths $B(E2)$ and reduced magnetic dipole transition strengths $B(M1)$. Most $B(M1)$ strengths were calculated assuming $\delta = 0$ (pure dipole decay) since they are rather insensitive to δ as long as it is small. Small values of δ have been observed systematically for mixed intraband $M1/E2$ transitions in several neighboring odd-odd nuclei, and are thus expected for similar transitions in ^{70}As. The one measured value of $\delta = 0.008(27)$ [9] that exists for a $\Delta J = 1$ transition in the yrast positive-parity band, corresponding to the 76.2-keV $9^+ \rightarrow 8^+$ transition, agrees with this assumption.

V. DISCUSSION

The lifetimes measured for the yrast positive-parity states indicate enhanced $B(E2)$ rates (see Table II) consistent with the expectation of a collective structure based on the $\pi g_{9/2} \otimes \nu g_{9/2}$ intrinsic configuration. Previous work has interpreted the associated high-spin rotational band within the context of the frequency evolution of the experimental kinematic moments of inertia, the signature splitting between adjacent spin states, and shape calculations using a cranked Woods-Saxon approach [10]. Since, however, the high-spin decays have been changed somewhat in this study, the kinematic moments of inertia and the signature-splitting pattern have been reinvestigated to see how these quantities may have been affected and how they now compare with those of neighboring odd-odd As isotopes. In addition, large-scale shell-model calculations were performed to see how well the collective features of this band could be reproduced from a more microscopic approach.

Coriolis mixing of the negative-parity orbitals tends to cloud the theoretical interpretation of negative-parity states at high spin. Nevertheless, the kinematic moments of inertia and signature-splitting pattern were also investigated for the lowest high-spin negative-parity states in order to characterize their behavior among similar structures throughout several proton-rich, odd-odd As isotopes. The results of these various interpretive calculations are described in the subsections below, following a brief description of the shell-model calculations that were performed.

A. Shell-model calculations

Shell-model (SM) calculations were performed for ^{70}As using the COSMO code [30] incorporating the $1p_{3/2}$, $0f_{5/2}$, $1p_{1/2}$, and $0g_{9/2}$ single-particle orbitals, and the JUN45 effective interaction [31]. Only positive-parity states were considered since the emphasis was on the calculation of high-spin yrast states with rather pure intrinsic configurations. Despite this restriction, a rich excitation spectrum was produced, consisting of 153 total states up to a maximum energy of 7.168 MeV (a non-yrast 15^+ state). However, two distinct sequences of yrast states emerged from this spectrum above the lowest 9^+ state, representing the lowest even- and odd-spin levels with $J > 9$. The mostly regular energy spacings between successive levels sharing the same signature implies an underlying rotational structure, supported by the enhanced $B(E2)$ rates predicted between states with $\Delta J = 2$ (see Sec. V D). These sequences were compared with the analogous positive-parity levels observed experimentally in a variety of ways, as discussed in the following subsections.

An overall comparison between the observed positive-parity states in ^{70}As above an excitation energy of 1000 keV and the corresponding states predicted by the SM calculations is illustrated in Fig. 6. The observed high-spin yrast states (which were grouped into two rotational bands in Fig. 1) are indicated in the first column of experimental levels, while the other measured states that are either known or assumed to have positive parity form the second column of states in the figure. The corresponding subset of states predicted by the SM calculations are arranged in similar fashion in the third and fourth columns. As seen in this level-scheme comparison, the SM calculations reproduce some of the observed states rather well, especially the 6^+ state which has a root-mean-square (rms) variance with the corresponding experimental level of only 62 keV. On the other hand, other predicted states show significant systematic differences with the experimental levels (rms deviations on the order of 1 MeV).

Focusing on the yrast high-spin levels (first and third columns of states in Fig. 6), the average rms variance between the experimental and theoretical excitation energies is 337 keV for states with $J > 8$, with a minimum (maximum) variance of 86 (649) keV for the 10^+ (13^+) state. In general, the SM calculations also predict the correct ordering of these levels. However, the lowest 8^+ (10^+) state is predicted to lie 1306 (396) keV above the yrast 9^+ (11^+) state, but experimentally it is observed to be 76 (153) keV below the lowest 9^+

(11^+) state.

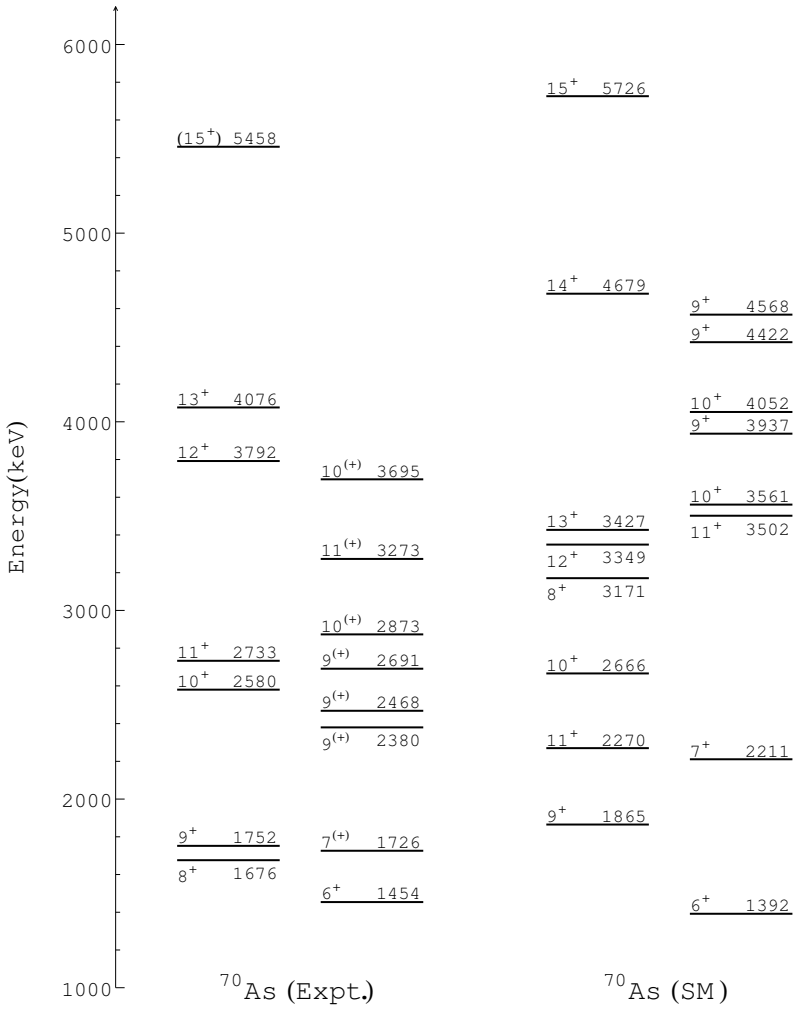

FIG. 6: Experimental and theoretical (as predicted by shell-model (SM) calculations) positive-parity level schemes for ^{70}As above an excitation energy of 1000 keV. The observed high-spin yrast states (which were grouped into two rotational bands in Fig. 1) are indicated in the first column of experimental levels, while the other measured states that are either known or assumed to have positive parity form the second column of states. The corresponding subset of states predicted by the SM calculations are arranged in similar fashion in the third and fourth columns.

B. Kinematic moments of inertia

Kinematic moments of inertia $J^{(1)}$ were calculated from the rotational model as a function of rotational frequency. The experimental values for the lowest positive- and negative-parity

sequences with signature $\alpha = 0$ and $\alpha = 1$ in ^{68}As [2], ^{70}As, ^{72}As [3], and ^{74}As [32] are shown in Fig. 7. Previously, the behavior of the $J^{(1)}$ values for the yrast positive-parity band in ^{70}As (see Fig. 3 in Ref. [10]) was very similar to that shown for ^{74}As in Fig. 7, having a rather smooth convergence toward a nearly constant value of about 25 $\hbar^2$/MeV with increasing frequency. Such a trend is typical of odd-odd nuclei in the $A \sim 80$ region [11, 33]. With the changes to the high-spin decays instituted in this work, however, the $J^{(1)}$ spectrum for the yrast positive-parity states in ^{70}As now seems to more strongly resemble that of ^{72}As, including an upturn in the pattern near $\hbar\omega \approx 0.6$ MeV for the $\alpha = 1$ sequence. This upturn is probably not associated with a qp alignment, since both a quasi-proton and quasi-neutron alignment are Pauli-blocked for the yrast positive-parity states. Rather, it could be a consequence of the γ-soft shapes associated with the lowest positive-parity configurations, as determined from previous total Routhian surface (TRS) calculations for both ^{70}As [10, 14] and ^{72}As [3]. Conversely, pronounced triaxial minima develop in the potential energy surfaces based on Cranked Nilsson-Strutinsky model calculations for the lowest high-spin positive-parity states in ^{74}As [32], which might account for the more consistent $J^{(1)}$ values in the same frequency range. The rather anomalous behavior of the $J^{(1)}$ values for the lowest positive-parity states in ^{68}As could be due to the lack of a regular $E2$ band built on the yrast $9^{(+)}$ state, suggested to be lowest member of the $\pi g_{9/2} \otimes \nu g_{9/2}$ configuration [2].

Superimposed in the top panel of Fig. 7 are the $J^{(1)}$ values inferred from the energies and spins of the yrast positive-parity states in ^{70}As predicted by the SM calculations. The magnitude of these values are similar to the experimental ones over the range of frequencies in which the two overlap, although the upturn in the experimental pattern for the $\alpha = 1$ sequence near $\hbar\omega \approx 0.6$ MeV is not reproduced by the SM calculations. The theoretical $J^{(1)}$ spectrum for the $\alpha = 1$ sequence also extends across a wider range of values (and frequencies) over the same spin range in which the experimental values were determined, reflecting a larger difference between the measured and predicted $E2$ transition energies near the top and bottom of this band.

The negative-parity $J^{(1)}$ spectra for $^{68-74}$As are considerably more complex, as indicated in the lower panel of Fig. 7, presumably due (at least in part) to qp alignments. In particular, the sharp backbends that occur in the $J^{(1)}$ curves for both signatures of the lowest negative-parity sequences in ^{70}As near $\hbar\omega \approx 0.6$ MeV are likely associated with band crossings that evidently result in increased collectivity for the favored band above the crossing (see Sec. IV).

Similar backbends are also observed in the $J^{(1)}$ spectra for the lowest negative-parity states in ^{68}As and ^{74}As, although the frequencies at which the backbends occur vary somewhat. In this regard, the yrast negative-parity states in ^{70}As appear to be more similar to the analogous structures in these nuclei than in ^{72}As, which shows little if any evidence of a backbend in the negative-parity structures. Still, the $J^{(1)}$ values for negative-parity states in ^{72}As should be interpreted with caution since they do not extend to as high a frequency as they do for the other nuclei shown in the figure. Moreover, the degree of collectivity for the yrast negative-parity sequences in $^{68-74}$As have yet to be quantified through lifetime measurements, making the interpretation of $J^{(1)}$ as the appropriate moment-of-inertia parameter for these structures somewhat unclear.

C. Signature splitting

The normalized energy differences between states differing in spin by $\Delta J = 1$ as a function of the upper-state spin J_i in the lowest positive- and negative-parity band sequences for the odd-odd $^{68-74}$As isotopes are shown in Fig. 8. Such energy differences are indicative of the degree of signature splitting between the favored and unfavored decay sequences of a given intrinsic configuration and tend to be sensitive to underlying structural properties. As demonstrated in the top panel of this figure, the alternating pattern associated with the yrast positive-parity band in ^{70}As seems most similar (in phase and magnitude) to the ones corresponding to the analogous decay sequences in ^{68}As [2] and ^{72}As [3]. Moreover, if one were to interpret the $J = 8$ level at 2474 keV in ^{68}As as the suspected [2] yrast 8^+ state, then even the magnitudes of the alternating patterns for ^{70}As and ^{68}As would be quite similar over the entire spin range for which the energy differences can be compared (although this 8^+ state in ^{68}As would lie above the lowest 9^+ state, unlike the situation in ^{70}As).

Good agreement was also observed in general between the signature-splitting pattern predicted by SM calculations and the experimental one for the yrast positive-parity states in ^{70}As, particularly for the states with $J_i = 10$ and 12, as indicated in the top panel of Fig. 8. This agreement, however, is more a reflection of the accuracy with which the SM calculations reproduce the relative energy spacings between adjacent levels, rather than the absolute excitation energies of each individual state (see Sec. V A and Fig. 6).

The rather large alternations above $J_i \gtrsim 9$, with the odd-spin states being energetically

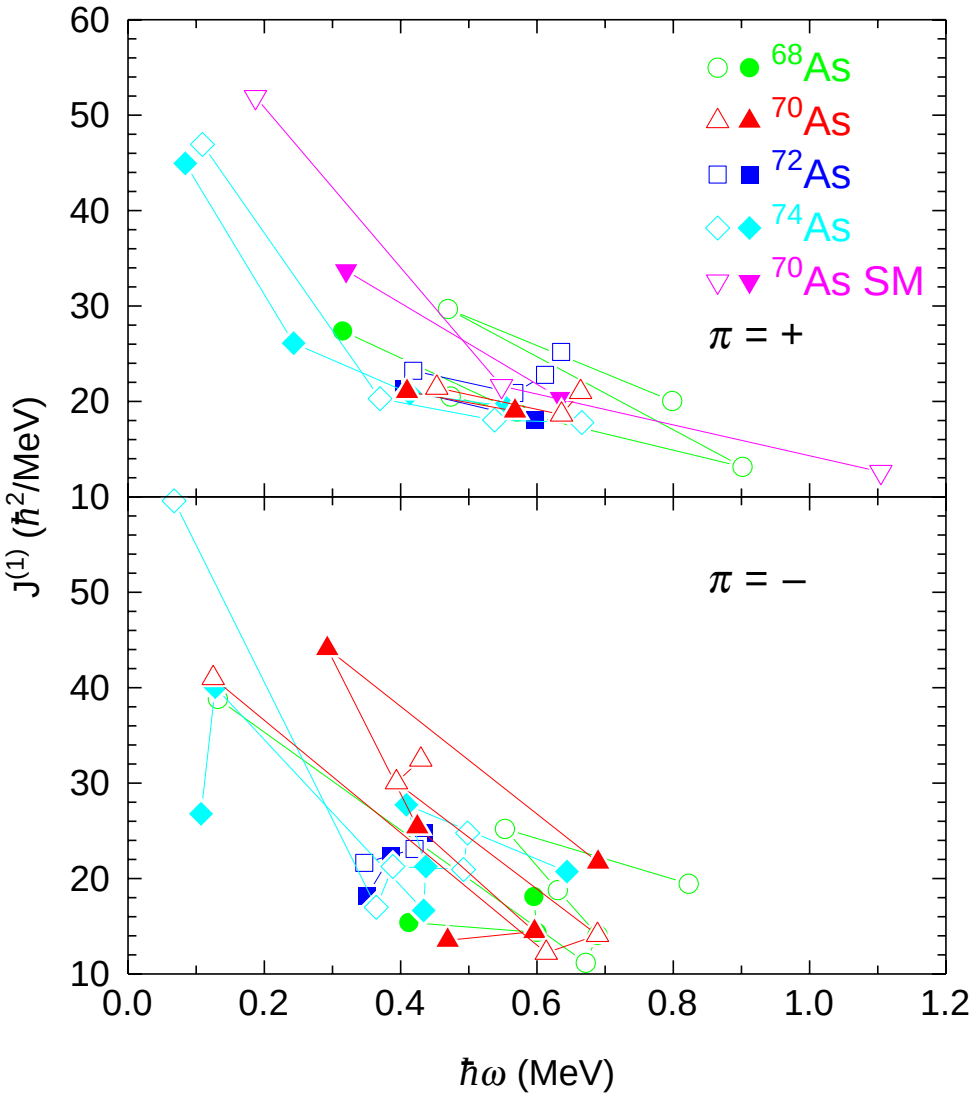

FIG. 7: (Color online) Experimental kinematic moments of inertia $J^{(1)}$ as a function of rotational frequency for the yrast positive- and negative-parity decay sequences in ^{68}As [2], ^{70}As, ^{72}As [3], and ^{74}As [32]. The $J^{(1)}$ values inferred from the energies and spins of the yrast positive-parity states in ^{70}As as predicted by shell-model (SM) calculations are also included in the top panel. Filled (open) symbols are used for sequences with signature $\alpha = 0$ ($\alpha = 1$). A common value of $K = 4$ was used for the spin-projection quantum number in each sequence except for the negative-parity bands in ^{74}As, in which $K = 2$ was used.

favored, has been explained [12] for structures based on the $\pi g_{9/2} \otimes \nu g_{9/2}$ configuration in terms of angular momentum generated exclusively by collective rotation once the spins of the two unlike $g_{9/2}$ nucleons become fully aligned with the core spin near $J \approx 9$ (the maximum

angular momentum generated by the unpaired proton and neutron). The collective nature of this band in ^{70}As has been verified and extended to higher spin in this work, and previous lifetime measurements in ^{72}As [3] have indicated a similar degree of collectivity in the same spin range (see Sec. V D). As mentioned in Sec. V B, however, a regular $E2$ band was not observed for the yrast positive-parity states in ^{68}As, despite TRS calculations that predicted a sequence of collective states at a triaxial deformation of $\beta_2 \approx 0.27$ and $\gamma \approx 22^\circ$ [2]. The SM calculations also predicted collective $E2$ transitions between yrast positive-parity states with $J_i > 10$ in ^{70}As (see Sec. V D). This is consistent with the picture of large alternations in the signature-splitting pattern revealed by these calculations in the same spin range.

Below $J \approx 9$, the two-qp-plus-rotor calculation of Ref. [12] suggests that angular momentum is generated by both collective rotation and a realignment of qp spins, manifested by a reversal in the phase of the alternating pattern such that the even-spin states now lie relatively lower in energy than the odd-spin ones. The fact that the alternating pattern does not continue below $J = 9$ in ^{70}As and has consistently large amplitudes at higher spins seems to be consistent with the interpretation [10] of two fully-aligned $g_{9/2}$ particles at the start of the band (representing a stretched $\pi g_{9/2} \otimes \nu g_{9/2}$ configuration), considering the predictions of the two-qp-plus-rotor calculation described above. The predicted orbital occupancies associated with the yrast 9^+ state, determined from the SM calculations performed in this work, indicate approximately one neutron (1.33) and one proton (1.07) in the $g_{9/2}$ orbital, lending further support to this interpretation. Additionally, the SM calculations do not yield collective transitions below the yrast 9^+ state, suggesting that the collective structure terminates at the 9^+_1 level.

On the other hand, the degree of triaxiality could also affect the observed signature splitting variations, and could possibly account for the differences between the observed alternations in ^{70}As and ^{72}As [10]. In fact, the phase reversal in the alternating pattern at high spin in ^{74}As has been attributed to an unpaired band crossing associated with significant triaxiality [32]. However, the γ-soft shapes associated with the lowest positive-parity configurations determined from previous TRS calculations in ^{68}As [2], ^{70}As [10, 14] and ^{72}As [3] make it difficult to draw any conclusions about the relative importance of the γ shape parameter on the signature-splitting behavior. It's interesting to note that the current SM calculations for ^{70}As also predict the possible onset of a reversal in the phase of the alternating pattern beginning at the 15^+ state, perhaps indicating increased triaxiality

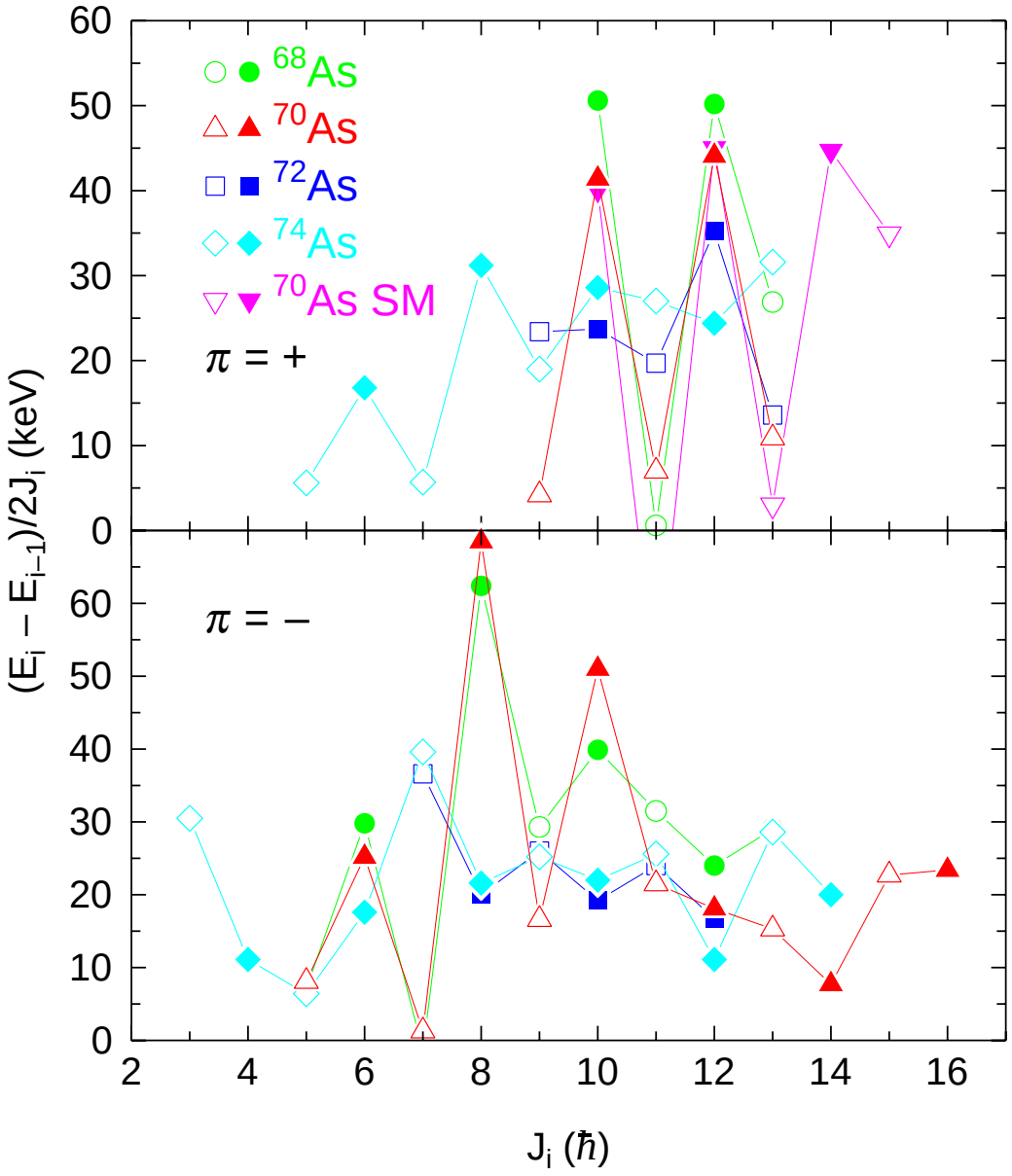

FIG. 8: (Color online) Normalized energy differences between adjacent states as a function of the spin J_i of the upper state for the yrast positive- and negative-parity decay sequences in ^{68}As [2], ^{70}As, ^{72}As [3], and ^{74}As [32]. Theoretical values predicted by shell-model (SM) calculations for the yrast positive-parity sequence in ^{70}As are also included in the top panel. Filled (open) symbols are used for states with even (odd) J_i.

as in ^{74}As. However, this predicted change in the staggering amplitude awaits experimental verification since the yrast 14^+ state has not yet been observed.

The signature-splitting patterns associated with the yrast negative-parity sequences also

reveal similarities among the same odd-odd As isotopes (bottom panel of Fig. 8), although they are much more difficult to interpret theoretically. Still, it seems clear that the pattern associated with ^{70}As is the most similar to that of ^{68}As over the spin range in which they can be compared, perhaps giving an indication of similar underlying structures.

D. Transition strengths

Theoretical $B(E2)$ and $B(M1)$ strengths were determined from the current SM calculations for transitions between the lowest positive-parity states in ^{70}As predicted by the calculations (third column of states in Fig. 6). The $E2$ transition operator invoked an effective neutron (proton) charge of 0.5 (1.5), adopted from previous f-p shell calculations [34]. $B(E2)$ and $B(M1)$ rates were also calculated between non-yrast positive-parity states, but the resulting values were usually significantly smaller than those corresponding to transitions between the yrast states. Some of these transitions could, however, correspond to those associated with the non-yrast positive-parity states observed experimentally.

When comparing the theoretical $B(E2)$ strengths with the experimental ones, as indicated in the top panel of Fig. 9, it becomes evident that the SM calculations systematically underestimate the degree of collectivity. Similar discrepancies have been observed for other f-p-g shell nuclei using the JUN45 effective interaction and have been attributed to the lack of incorporating the $f_{7/2}$ and $d_{5/2}$ orbitals into the model space [31]. The degree of quadrupole collectivity could be enhanced by increasing the neutron effective charge, but usually this comes at the cost of worsening the agreement between the predicted and measured excitation energies [31]. Furthermore, the somewhat steadily decreasing trend in $B(E2)$ with spin predicted by the SM calculations was not observed experimentally. (A theoretical $B(E2)$ rate is not included for the yrast $10^+ \rightarrow 8^+$ transition since the 8^+_1 state is predicted to lie above the 10^+_1 state in the calculations.)

The theoretical $B(M1)$ values of 0.028 μ_N^2 and 0.0063 μ_N^2 predicted for the 10^+_1 and 12^+_1 parent states, respectively, compare very favorably with the experimental ones, as illustrated by the strong overlap between the two sets of points in the bottom panel of Fig. 9. We did not compare the theoretical and experimental $B(M1)$ strengths for the yrast 9^+ and 11^+ parent-state transitions since the 8^+_1 (10^+_1) state lies above the 9^+_1 (11^+_1) state in the calculations (see Fig. 6).

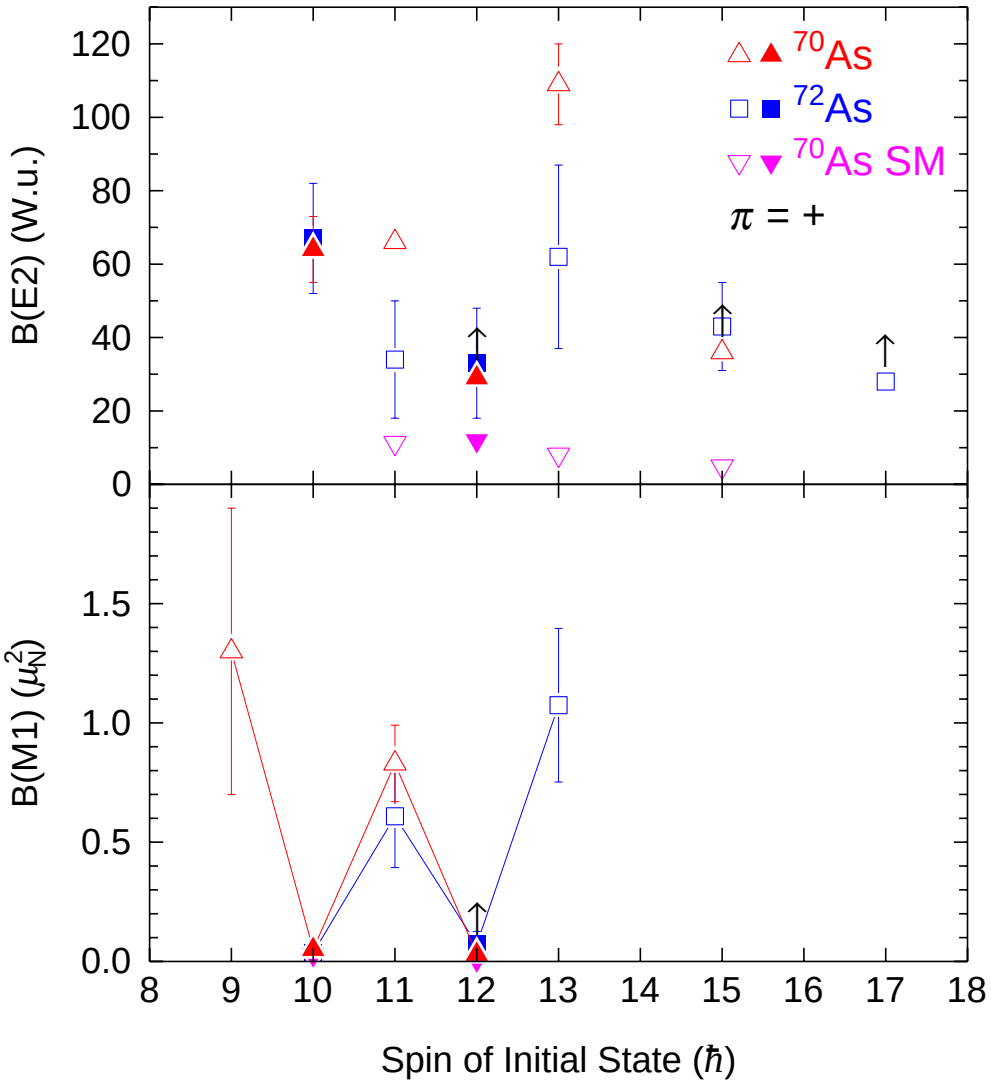

FIG. 9: (Color online) $B(E2)$ (top) and $B(M1)$ (bottom) strengths for transitions within the yrast positive-parity bands in ^{70}As and ^{72}As [3] as a function of the parent-state spin. Theoretical $B(E2)$ and $B(M1)$ values predicted by shell-model (SM) calculations for the yrast positive-parity sequences in ^{70}As are also included. Filled (open) symbols are used for states with even (odd) parent-state spin J_i. Symbols with arrows indicate lower limits established by effective-lifetime measurements. Some error bars are smaller than the symbol size. The experimental $B(M1)$ value for the $J_i = 9$ state in ^{70}As was inferred from a previous lifetime measurement [13].

Figure 9 also shows the $B(E2)$ and $B(M1)$ strengths measured within the yrast positive-parity band in ^{72}As [3], the only other neighboring odd-odd As isotope for which these results are available. These measurements show good agreement with the corresponding values in

^{70}As within experimental uncertainty, with the exception of the $B(E2)$ rates associated with the yrast 11^+ and 13^+ parent-state transitions in each nucleus. The strong alternations observed in the $B(M1)$ strengths for both nuclei are consistent in phase and magnitude with those of other odd-odd nuclei in this mass region [11]. They have been understood within the context of both the interacting boson-fermion approximation [35] and the two-qp-plus-rotor coupling model [36] in terms of how the odd particles couple to the core spin. A $\Delta J = 1$ decay from a favored signature ($\alpha = 1$) state involves only a realignment of the single-particle spin without altering the core spin and hence generates relatively strong $M1$ radiation. The corresponding decay originating from an unfavored signature ($\alpha = 0$) state requires a change in the core rotation (or boson number), which leads to reduced $B(M1)$ strength. Projected shell-model calculations performed for the yrast positive-parity band in odd-odd ^{80}Y [37] indicated that the $B(M1)$ staggering amplitudes are also sensitive to the underlying core deformation, and thus which orbitals lie closer to the Fermi level. When $g_{9/2}$ orbitals with smaller K components are closer to the Fermi level, their occupation leads to increased $B(M1)$ staggering amplitudes. The strong amplitudes seen in the $B(M1)$ alternations for ^{70}As thus seem to yield further evidence supporting a picture of a stretched $\pi g_{9/2} \otimes \nu g_{9/2}$ configuration for the yrast positive-parity band, since the occupation of low-K orbitals tends to provide a more rapid onset of spin alignment [10].

VI. SUMMARY

The high-spin decay of ^{70}As was studied using the ^{55}Mn(^{18}O,3n) reaction at a beam energy of 50 MeV using the John D. Fox Superconducting Accelerator Facility at Florida State University. The isotopically enriched ^{55}Mn target included a gold backing foil to stop all recoils and hence allowed for the measurement of lifetimes using the Doppler-shift attenuation method (DSAM). Prompt γ-γ coincidences were detected using a Compton-suppressed Ge array consisting of three Clover detectors and seven single-crystal detectors.

A thorough reinvestigation of the ^{70}As level scheme resulted in the assignment of 32 new transitions and a reassignment of 10 others when compared to the most recent published work. The intensities of all observed transitions in ^{70}As were measured, and spin-parity assignments were made based on directional correlation of oriented nuclei (DCO) ratios coupled with transition probability arguments. Modifications were made to the yrast positive-parity

band sequences, resulting in new 12^+ and (15^+) states. Significant changes were made to the negative-parity decay structure, supported by the observed coincidence relations, new linking transitions, and the measured γ-ray intensities. Several non-yrast states were observed within an excitation energy range of about 1700-3700 keV, and were tentatively assigned positive parity based on their decay to only the yrast positive-parity states and to each other.

The lifetimes of seven excited states were measured using the DSAM, with the experimental line shapes obtained at two separate detector angles. Five of the seven lifetimes represent new measurements, and the mean lifetime determined for the yrast 13^+ state replaces the upper limit known previously. The $B(E2)$ transition strengths inferred from the lifetimes measured in the yrast positive-parity band indicate a significant degree of collectivity for this structure, in agreement with the interpretations proposed in previous studies. In general, the $B(E2)$ strengths also show good agreement with those deduced for a similar structure in ^{72}As. Strong alternations were observed in the $B(M1)$ rates with spin in this band, very similar to that observed in ^{72}As and other odd-odd nuclei in this mass region.

Large-scale shell-model calculations were performed for ^{70}As using the JUN45 interaction and the $1p_{3/2}$, $0f_{5/2}$, $1p_{1/2}$, and $0g_{9/2}$ valence states in the f-p-g shell, and were used to predict the excitation energies as well as the $B(E2)$ and $B(M1)$ rates for transitions between the lowest high-spin yrast positive-parity states. Overall, the calculations reproduced the relative energy differences between adjacent spin states in this band rather well, resulting in generally good agreement with the experimental signature-splitting pattern and fair agreement with the inferred kinematic moments of inertia $J^{(1)}$. The level of agreement achieved with parameters associated with the excitation energies, however, came at the cost of systematically smaller $B(E2)$ rates predicted for this band structure. On the other hand, good agreement was achieved between the theoretical and experimental $B(M1)$ strengths where comparisons were made. More similarities than differences were observed in the signature-splitting patterns and $J^{(1)}$ spectra associated with the yrast positive-parity bands in the $^{68-74}$As odd-odd isotopes, although the signature-splitting ($J^{(1)}$) pattern for ^{70}As seems most similar to that of ^{68}As (^{72}As). The behavior of the signature-splitting pattern and $B(M1)$ alternations seem consistent with the interpretation of a stretched $\pi g_{9/2} \otimes \nu g_{9/2}$ configuration for the yrast positive-parity band beginning at the lowest 9^+ state, in agreement with the calculated $g_{9/2}$ orbital occupancies determined for the 9^+_1 state predicted by the

shell-model calculations.

Significantly more variation was observed in the signature-splitting patterns and $J^{(1)}$ spectra within the yrast negative-parity sequences among the odd-odd $^{68-74}$As isotopes, owing to the mixed intrinsic configurations involved in these structures. Despite these variations, the behaviors of the signature-splitting pattern and $J^{(1)}$ spectrum associated with these sequences in ^{70}As appear most similar to those related with the analogous structures in ^{68}As. The various similarities that ^{70}As shows with both ^{68}As and ^{72}As seems to underscore its transitional character as the neutron number evolves among the proton-rich odd-odd As isotopes.

Acknowledgments

This work was supported in part by the U. S. National Science Foundation through grants PHY-10-64819 (FSU) and PHY-1262850 (OWU), as well as the Ohio Wesleyan University Summer Science Research Program. Three authors (P.R.P.A., N.H.M., and J.R.B.O.) acknowledge financial support from the Brazilian agencies CNPq and FAPESP. We are grateful to the staff of the FSU John D. Fox Superconducting Accelerator Facility for their support throughout the experiment.

[1] K. Langanke, D. J. Dean, and W. Nazarewicz, Nucl. Phys. A **728**, 109 (2003).

[2] E. A. Stefanova, K. P. Lieb, I. Stefanescu, G. De Angelis, D. Curien, J. Eberth, E. Farnea, A. Gadea, G. Gersch, A. Jungclaus, T. Martinez, R. Schwengner, T. Steinhardt, N. Warr, D. Weisshaar, and R. Wyss, Eur. Phys. J. A **24**, 1 (2005).

[3] J. Döring, S. L. Tabor, J. W. Holcomb, T. D. Johnson, M. A. Riley, and P. C. Womble, Phys. Rev. C **49**, 2419 (1994).

[4] J. Döring, D. Pantelică, A. Petrovici, B. R. S. Babu, J. H. Hamilton, J. Kormicki, Q. H. Lu, A. V. Ramayya, O. J. Tekyi-Mensah, and S. L. Tabor, Phys. Rev. C **57**, 97 (1998).

[5] B. O. ten Brink, R. D. Vis, A. W. B. Kalshoven, and H. Verheul, Z. Phys. **270**, 83 (1974).

[6] B. O. ten Brink, J. Akkermans, P. van Nes, and H. Verheul, Nucl. Phys. A **330**, 409 (1979).

[7] Zs. Podolyák, T. Fényes, and J. Timár, Nucl. Phys. A **584**, 60 (1995).

[8] A. Filevich, M. Behar, G. García Bermúdez, M. A. J. Mariscotti, E. Der Mateosian, and P. Thieberger, Nucl. Phys. A **309**, 285 (1978).

[9] T. Bădică, V. Cojocaru, D. Pantelică, I. Popescu, and N. Scîntei, Nucl. Phys. A **535**, 425 (1991).

[10] B. Mukherjee, G. Mukherjee, P. Joshi, R. P. Singh, S. Muralithar, A. K. Pande, L. Chaturvedi, S. C. Pancholi, and R. K. Bhowmik, Acta Phys. Hung. New Ser.: Heavy Ion Phys. **11**, 305 (2000).

[11] S. L. Tabor, Acta Phys. Hung. New Ser.: Heavy Ion Phys. **2**, 239 (1995).

[12] A. J. Kreiner and M. A. J. Mariscotti, Phys. Rev. Lett. **43**, 1150 (1979).

[13] C. Morse, H. Iwasaki, A. Lemasson, T. Baugher, D. Bazin, J. S. Berryman, A. Dewald, C. Fransen, A. Gade, S. McDaniel, A. J. Nichols, A. Ratkiewicz, S. R. Stroberg, P. Voss, R. Wadsworth, D. Weisshaar, K. Wimmer, and R. Winkler, Phys. Rev. C **90**, 034310 (2014).

[14] G. García Bermúdez, J. Döring, G. D. Johns, R. A. Kaye, M. A. Riley, S. L. Tabor, C. J. Gross, M. J. Brinkman, and H. Q. Jin, Phys. Rev. C **56**, 2869 (1997).

[15] J. Pavan, Ph. D. thesis, Florida State University, 2003.

[16] `[http://fsunuc.physics.fsu.edu/~caussyn/]`.

[17] Table of Isotopes, ed. R. B. Firestone and V. S. Shirley, eighth edition (Wiley-Interscience, New York, 1996).

[18] E. F. Moore, P. D. Cottle, C. J. Gross, D. M. Headly, U. J. Hüttmeier, S. L. Tabor, and W. Nazarewicz, Phys. Rev. C **38**, 696 (1988).

[19] H. A. Helms, G. J. Zaal, W. Hogervorst, and J. Blok, Hyperfine Int. **2**, 399 (1976).

[20] W. Hogervorst, H. A. Helms, G. J. Zaal, J. Bouma, and J. Blok, Z. Phys. A **294**, 1 (1980).

[21] M. Sugawara, Y. Toh, M. Oshima, M. Koizumi, A. Kimura, A. Osa, Y. Hatsukawa, H. Kusakari, J. Goto, M. Honma, M. Hasegawa, and K. Kaneko, Phys. Rev. C **81**, 024309 (2010).

[22] B. Mukherjee, S. Muralithar, G. Mukherjee, R. P. Singh, R. Kumar, J. J. Das, P. Sugathan, N. Madhavan, P. V. Madhusudanan Rao, A. K. Sinha, G. Shanker, S. L. Gupta, D. Mehta, S. L. Katoch, C. R. Praharaj, A. K. Pande, L. Chaturvedi, S. C. Pancholi, and R. K. Bhowmik, Acta Phys. Hung. New Ser.: Heavy Ion Phys. **13**, 253 (2001).

[23] `[http://www.srim.org]`.

[24] G. Cowan, *Statistical Data Analysis* (Oxford University Press, New York, 1998).

[25] J. R. Taylor, *An Introduction to Error Analysis: The Study of Uncertainties in Physical Measurements* (University Science Books, Sausalito, 1997).

[26] R. A. Kaye, C. J. Drover, S. L. Tabor, J. Döring, Y.-C. Yang, Y. Sun, S. R. Arora, N. R. Baker, J. K. Bruckman, T. A. Hinners, C. R. Hoffman, and S. Lee, Phys. Rev. C **83**, 044316 (2011).

[27] F. Cristancho and K. P. Lieb, Nucl. Phys. A **486**, 353 (1988).

[28] S. L. Tabor, J. Döring, J. W. Holcomb, G. D. Johns, T. D. Johnson, T. J. Petters, M. A. Riley, and P. C. Womble, Phys. Rev. C **49**, 730 (1994).

[29] F. Cristancho, K. P. Lieb, J. Heese, C. J. Gross, W. Fieber, Th. Osipowicz, S. Ulbig, K. Bharuth-Ram, S. Skoda, J. Eberth, A. Dewald, and P. von Brentano, Nucl. Phys. A **501**, 118 (1989).

[30] `[http://www.volya.net/index.php?id=cosmo]`.

[31] M. Honma, T. Otsuka, T. Mizusaki, and M. Hjorth-Jensen, Phys. Rev. C **80**, 064323 (2009).

[32] Shi-Peng Hu, Hai-Liang Ma, Xue-Peng Cao, Xiao-Guang Wu, Huan-Qiao Zhang, Hui Hua, Jun-Jie Sun, Hui-Bin Sun, Chuang-Ye He, Yun Zheng, Guang-Sheng Li, Cong-Bo Li, Shun-He Yao, Bei-Bei Yu, Jin-Long Wang, Hong-We Li, Yi-Heng Wu, Jia-Jian Liu, Peng-Wei Luo, Chuan Xu, Yi-Yuan Cheng, Phys. Lett. B **732**, 59 (2014).

[33] S. L. Tabor, Phys. Rev. C **45**, 242 (1992).

[34] M. Honma, T. Otsuka, B. A. Brown, and T. Mizusaki, Phys. Rev. C **69**, 034335 (2004).

[35] P. Chowdhury, C. J. Lister, D. Vretenar, Ch. Winter, V. P. Janzen, H. R. Andrews, D. J. Blumenthal, B. Crowell, T. Drake, P. J. Ennis, A. Galindo-Uribarri, D. Horn, J. K. Johansson, A. Omar, S. Pilotte, D. Prévost, D. Radford, J. C. Waddington, and D. Ward, Phys. Rev. Lett. **67**, 2950 (1991).

[36] P. C. Womble, J. Döring, T. Glasmacher, J. W. Holcomb, G. D. Johns, T. D. Johnson, T. J. Petters, M. A. Riley, V. A. Wood, S. L. Tabor, and P. Semmes, Phys. Rev. C **47**, 2546 (1993).

[37] R. A. Kaye, O. Grubor-Urosevic, S. L. Tabor, J. Döring, Y. Sun, R. Palit, J. A. Sheikh, T. Baldwin, D. B. Campbell, C. Chandler, M. W. Cooper, S. M. Gerbick, C. R. Hoffman, J. Pavan, L. A. Riley, and M. Wiedeking, Phys. Rev. C **69**, 064314 (2004).

[38] `[http://bricc.anu.edu.au/]`.

TABLE I: Energies, spin-parity assignments for the initial and final state, relative intensities (I_γ), DCO ratios ($R_{\rm DCO}$), multipolarities (σL), and parent-level energies associated with the transitions assigned to ^{70}As.

E_γ (keV)	J_i^π	J_f^π	I_γ[1]	$R_{\rm DCO}$	σL	$E_{\rm Lev}$ (keV)
18.3[2]	7^-	6^-			$M1/E2$	887.8(2)
32.1(1)[2]	2^+	4^+	> 1.5[2]		$E2$	32.1(1)[2]
76.2(1)	9^+	8^+	64(10)[3]	0.56[4]	$M1/E2$	1752.2(2)
81.2(1)	5^-	4^-	148(12)		$M1/E2$	566.7(1)
95.0(2)	4^-	3^+	3.8(6)		$E1$	485.5(1)
134.7(2)	3^+	2^+	87(4)		$M1/E2$	166.8(1)
153.0(3)	11^+	10^+	2.0(4)		$M1/E2$	2733.0(3)
166.8(1)	3^+	4^+	22.1(11)		$M1/E2$	166.8(1)
221.8(4)	8^+	6^+	1.4(4)		$E2$	1676.0(2)
223.4(4)	3^+	3^+	2.4(8)		$M1/E2$	390.2(4)
271.8(3)	$7^{(+)}$	6^+	2.4(3)	0.49(10)	$(M1/E2)$	1726.0(4)
302.8(1)	6^-	5^-	31(2)	1.47(31)[5]	$M1/E2$	869.5(1)
312.0(6)		6^+	1.3(4)			1765.6(4)
318.9(2)	4^-	3^+	90(9)	0.65(14)	$E1$	485.5(1)
321.1(2)	7^-	5^-	113(11)	1.16(18)	$E2$	887.8(2)
331.8(2)	(5)	5^-	2.0(9)			898.5(2)
398.0(1)	13^-	12^-	3.2(4)	0.46(9)	$M1/E2$	4605.0(3)
406.1(4)	$10^{(+)}$	$9^{(+)}$	0.6(4)		$(M1/E2)$	2873.3(4)
408.2(3)	6^+	6^-	1.8(4)		$E1$	1454.2(2)
479.2(1)	6^-	5^-	11.3(4)	0.87(10)	$M1/E2$	1045.9(1)
485.5(1)	4^-	4^+	72(4)	0.87(2)	$E1$	485.5(1)
490.3(4)	13^-	11^-	2.8(10)		$E2$	4605.0(3)
566.4(1)	6^+	7^-	9.9(8)	0.48(5)	$E1$	1454.2(2)
596.3(3)	9^-	8^-	11(3)	0.55(18)	$M1/E2$	2579.5(3)

612.3(3)	14^-	12^-	10(2)	0.92(11)	$E2$	4819.4(6)
626.9(2)	7^-	6^-	9.4(9)	0.88(14)[6]	$M1/E2$	1496.4(2)
693.2(3)	$11^{(+)}$	10^+	9(2)	0.27(6)	$(M1/E2)$	3273.2(3)
703.5(8)	$9^{(+)}$	8^+	1.6(5)	1.24(29)[5]	$(M1/E2)$	2379.6(5)
719.5(5)		6^-	1.2(5)			1765.6(4)
741.5(8)	$9^{(+)}$	$7^{(+)}$	2.2(10)		$(E2)$	2467.5(9)
743.2(2)	14^-	13^+	7.1(10)	0.56(3)	$E1$	4819.4(6)
759.9(6)	(14^-)	13^-	2.2(9)	0.18(7)	$(M1/E2)$	(5365.4)
771.5(8)	9^-	7^-	1.0(3)	1.02(22)	$E2$	2579.5(3)
788.2(1)	8^+	7^-	100(3)[7]	0.44(1)	$E1$	1676.0(2)
791.5(9)	$9^{(+)}$	8^+	7(2)	0.52(6)[5]	$(M1/E2)$	2467.5(9)
805.1(4)	$11^{(+)}$	$9^{(+)}$	3.5(10)		$(E2)$	3273.2(3)
812.1(3)	13^-	12^+	1.6(4)	0.47(6)	$E1$	4605.0(3)
827.9(3)	10^+	9^+	13(2)	1.21(34)[5]	$M1/E2$	2580.0(3)
832.4(3)	13^-	11^-	13(3)	1.10(10)	$E2$	4605.0(3)
893.9(4)	15^-	13^-	9(2)	0.87(10)	$E2$	5498.9(5)
896.4(6)		6^-	5.2(10)			1765.6(4)
904.0(4)	10^+	8^+	20(5)	0.80(17)	$E2$	2580.0(3)
905.7(6)	12^-	10^-	7(2)	1.27(18)	$E2$	4207.0(3)
919.0(4)	7^-	7^-	5.0(10)	0.81(8)	$M1/E2$	1806.8(4)
929.6(4)	7^-	5^-	5.8(18)	0.91(31)	$E2$	1496.4(2)
934.1(8)	12^-	$11^{(+)}$	0.6(3)		$(E1)$	4207.0(3)
938.4(6)	8^-	6^-	4.7(14)	0.83(22)	$E2$	1984.2(3)
980.7(3)	11^+	9^+	47(4)	0.95(14)	$E2$	2733.0(3)
1015.1(3)	$9^{(+)}$	8^+	6.0(12)	0.35(10)	$(M1/E2)$	2691.1(4)
1058.9(6)	12^+	11^+	4.6(14)	0.68(14)	$M1/E2$	3792.0(5)
1065.3(5)	$15^{(-)}$	14^-	2.5(8)	0.64(18)	$(M1/E2)$	5884.7(8)
1081.9(5)	9^-	7^-	5.8(16)	1.62(28)	$E2$	2579.5(3)
1114.7(4)	8^-	6^-	15.6(15)	0.84(20)	$E2$	1984.2(3)
1121.1(4)	$10^{(+)}$	9^+	6.1(15)	0.30(10)	$(M1/E2)$	2873.3(4)

1159.2(8)	(14^-)	12^-	1.8(8)		$(E2)$	(5365.4)
1194.0(8)	11^-	9^-	4.0(10)	0.88(23)	$E2$	3773.5(9)
1212.0(6)	12^+	10^+	12(4)	0.85(16)	$E2$	3792.0(5)
1227.3(10)	$10^{(+)}$	$9^{(+)}$	4.3(10)	0.50(12)	$(M1/E2)$	3694.8(13)
1317.0(7)	10^-	8^-	7.4(15)	1.26(26)	$E2$	3301.2(8)
1343.3(6)	13^+	11^+	19(2)	0.96(5)	$E2$	4076.3(7)
1381.8(8)	(15^+)	13^+	3.9(15)		$(E2)$	5458.1(11)
1394.4(3)	9^-	7^-	15(2)	0.88(10)	$E2$	2282.2(4)
1427.7(6)	(16^-)	14^-	1.9(9)		$(E2)$	6247.1(8)
1454.2(8)	6^+	4^+	1.3(6)		$E2$	1454.2(2)
1474.0(3)	12^-	11^+	6.2(9)	0.55(4)	$E1$	4207.0(3)
1490.0(3)	11^-	9^-	9.0(15)	0.80(15)	$E2$	3773.5(9)
1521.3(8)	$11^{(+)}$	9^+	3.0(5)		$(E2)$	3273.2(3)
1832.8(10)	11^-	9^-	1.3(6)		$E2$	4115.5(7)

[1] Determined at 90° and corrected for angular distribution effects (see text) unless otherwise noted.
[2] From Ref. [9].
[3] Determined at 35° and corrected for angular distribution effects (see text).
[4] From Ref. [10].
[5] Obtained by gating on the 788.2-keV $E1$ transition.
[6] Obtained by gating on the 318.9-keV $E1$ transition.
[7] Intensities normalized to this transition.

TABLE II: γ-ray branching ratios R_B, lifetimes, and reduced transition strengths in ^{70}As. Individual lifetimes deduced from a DSAM analysis of line shapes measured at the indicated angles from transitions with energy E_γ are given in the same row. The accepted lifetimes ($\tau_{\rm acc}$) represent the weighted average (based on the uncertainties) of the measurements at 35° and 145° where results are available.

$E_{\rm Lev}$ (keV)	J_i^π	E_γ (keV)	R_B (%)	$\tau_{\rm prev}$[1] (ps)	$\tau_{35°}$ (ps)	$\tau_{145°}$ (ps)	$\tau_{\rm acc}$ (ps)	$B(E2)$ (W.u.)[2]	$B(M1)$ (μ_N^2)
1676.0	8^+	788.2	98.6(4)	80(29)[3]			80(29)[3]		$1.6(6)\times10^{-5}$[4]
		221.8	1.4(4)					15.5(9)	
1752.2	9^+	76.2	100[5]	85(43)[3]			85(43)[3]		1.3(6)[6]
2580.0	10^+	904.0	62(7)		0.80^{+10}_{-8}	0.73^{+9}_{-8}	0.76(6)	64(9)	
		827.9	38(7)						0.050(10)
2733.0	11^+	980.7	95.9(8)	1.1(3)[7]	0.75^{+3}_{-2}	0.77(2)	0.76(2)	66(2)	
		153.0	4.1(8)						0.83(16)[8]
3792.0	12^+	1212.0	72(10)		<0.41[9]	<0.47[9]	<0.45[9]	>29	
		1058.9	28(10)						>0.030
4076.3	13^+	1343.3	100	<0.6[7]	0.11(1)	0.09(1)	0.10(1)	109(11)	
4207.0	12^-	1474.0	44(7)			<1.10[9]	<1.10[9]		$>7.9\times10^{-5}$[10]
		934.1	4(2)						$>2.8\times10^{-5}$[10]
		905.7	52(7)					>37	
4819.4	14^-	743.2	42(6)			<3.20[9]	<3.20[9]		$>2.0\times10^{-4}$[10]
		612.3	58(6)					>100	
5458.1	(15^+)	1381.8	100		<0.22[9]	<0.28[9]	<0.26[9]	>36	

[1] Lifetimes measured from previous work as indicated in the table.
[2] 1 W.u. = 17.14 e^2fm^4.
[3] From Ref. [13].
[4] $B(E1)$ in e^2fm^2 using a dipole-quadrupole mixing ratio $\delta = 0.017(13)$[9] and the γ-ray branching ratio

determined in this work.

[5] Transition branching ratio including both γ-ray and electron conversion branching.

[6] Calculated using $\delta = 0.008(27)$[9], an $M1$ internal conversion coefficient $\alpha_T(M1) = 0.190(4)$[38], and an $E2$ internal conversion coefficient $\alpha_T(E2) = 2.172$[38].

[7] From Ref. [14].

[8] Calculated using $\delta = 0$ and an $M1$ internal conversion coefficient $\alpha_T(M1) = 0.0288(5)$[38].

[9] Effective lifetime.

[10] $B(E1)$ in $e^2\text{fm}^2$ assuming $\delta = 0$.